Available online at www.sciencedirect.com
SCIENCE DIRECT®
International Journal of Heat and Mass Transfer 47 (2004) 3145–3157
International Journal of HEAT and MASS TRANSFER
www.elsevier.com/locate/ijhmt

Thermal end effects on electroosmotic flow in a capillary

Xiangchun Xuan, David Sinton, Dongqing Li *

Department of Mechanical and Industrial Engineering, University of Toronto, 5, King's College Road, Toronto, Ont., Canada M5S 3G8

Received 21 May 2003; received in revised form 13 February 2004
Available online 17 April 2004

Abstract

Thermal end effects on electroosmotic flow in a capillary are numerically investigated in this paper. The model accounts for the dynamic coupling effects of Joule heating on the temperature field, the electrical double layer field, the applied electric potential field and the flow field in the full capillary from reservoir to reservoir. These fields are strongly coupled via temperature dependent liquid properties. We find the electric field intensity is non-uniform due to reservoir-based thermal end effects. The resulting cross-stream velocity profile is concave near the inlet and outlet regions, and convex through the central portion of the capillary. These deviations from ideal electroosmotic flow are induced by axial temperature gradients. The calculated liquid temperature lies between the values predicted by previous "solid" solution models with constant and the models with variable electric conductivities, and is in qualitative agreement with experimental observations. The influence of various working parameters (including applied electric field, ionic concentration, zeta potential) and also the capillary size (including diameter and length) is investigated.

1. Introduction

Electroosmosis describes the motion of bulk liquid with respect to a charged solid surface in response to an electric field applied parallel to the surface [1]. Electroosmotic flow offers many advantages over the more conventional pressure-driven flow; in that no moving parts are required, the plug-like velocity profile reduces dispersion of discrete samples, and it is well suited to miniaturization. The advent of microfabricated fluidic devices has seen many applications of electroosmotic flow. It has been extensively used to "pump" the solution through either a capillary [2] or a channel micromachined in a chip [3] during electrophoresis. It is also a method of controlling the sample injections in microchips [4,5]. However, there exists an inevitable Joule heating effect accompanying the electroosmotic flow, especially significant when high voltages are applied. This effect produces temperature gradients in both cross-stream and axial directions in the channel, of which the former has been extensively studied and long understood to cause the band spreading of charged analytes and thus a reduction in the separation efficiency [6–9]. In addition, elevated solution temperatures can lead to denaturation of proteins or nucleic acids [10]. The use of glass microfluidic chips greatly mitigates Joule heating effects through rapid heat conduction and thermal inertia. However, increasingly popular polymer-based (e.g., PDMS) chips, which can have a very low thermal conductivity, can suffer from Joule heating effects significantly. Therefore, it remains important to control the liquid temperature in microfluidic systems.

A variety of experimental techniques have been developed to measure the liquid temperature inside microfluidic systems, like backscatter interferometry [11], nuclear magnetic resonance (NMR) [12], Raman spectroscopy [13], and temperature sensitive probes (e.g., thermochromic liquid crystal [14], phosphorescent [15] or fluorescent dye [16,17] etc.). Using caged-dye based flow visualization, Sinton and Li [18] found a slight curvature in the electroosmotic velocity profiles obtained at the capillary middle point. Although the presence of the curvature was shown to correlate with

* Corresponding author. Tel.: +1-416-978-1282; fax: +1-416-978-7753.
E-mail address: dli@mie.utoronto.ca (D. Li).

0017-9310/$ - see front matter © 2004 Elsevier Ltd. All rights reserved.
doi:10.1016/j.ijheatmasstransfer.2004.02.023

Nomenclature

C	molar concentration (mol l^{-1})
C_p	specific heat
e	electron charge, 1.602×10^{-19} C
$\mathbf{E}$	applied electric field
h	heat transfer coefficient
k	thermal conductivity
K_B	Boltzmann's constant, 1.381×10^{-23} J K^{-1}
n_0	bulk ionic concentration (m^{-3})
N_a	Avogadro's number, 6.022×10^{23} mol^{-1}
p	hydrodynamic pressure
P	non-dimensional pressure
P_e	Peclet number
R	capillary radius
t	Time
T	absolute temperature
T_∞	ambient temperature, 298 K
$\mathbf{v}$	velocity vector
$\mathbf{V}$	non-dimensional velocity vector
z_v	valence of ions

Greek symbols

σ	electric conductivity
ε	dielectric constant
ε_0	permittivity of the vacuum, 8.854×10^{-12} C V^{-1} m^{-1}
κ	Debye–Huckel parameter (m^{-1})
λ	molar conductivity
μ	dynamic viscosity
ϕ	external potential field
Φ	non-dimensional electric field
ψ	internal potential field
ρ	mass density (kg m^{-3})
ρ_e	electric charge density (C m^{-3})
τ	non-dimensional time
Θ	non-dimensional temperature
ζ	zeta potential

Subscripts

p	parameters associated with polyimide coating
ref	reference parameters
w	parameters associated with capillary wall

expected Joule heating effects, the exact mechanism was not determined. Also, quite a few researchers have carried out theoretical analyses to calculate the liquid temperature. Grushka et al. [6] and Knox [8] assumed a constant electric conductivity of the solution, and obtained a radially parabolic temperature profile. Gobbie and Ivory [19] and Bello and Righetti [20] pointed out that assuming a constant electric conductivity resulted in underestimated liquid temperatures because in reality, conductivity increases with temperature. In these previous analyses, the solution was viewed as a "solid" conductor and the advective effects of electroosmotic flow were neglected, as were the thermal end effects due to the presence of reservoirs. Moreover, they did not consider the dynamic change of electric field intensity when the electric conductance of solutions varied with temperature. We will show in this work that the real liquid temperature is an intermediate value between the two temperatures predicted by the "solid" solution models with and without accounting for the temperature dependence of electric conductivity.

The flow field, electric potential field and temperature field are strongly coupled if the temperature dependence of electric conductivity is taken into consideration. Computer aided numerical simulation is the only option to solve this problem. A number of simulations have been conducted on these coupled fields. Zhao and Liao [21] analyzed the thermal effects on electroosmotic pumping of liquids in a slit channel, but they assumed a constant electric field and imposed isothermal conditions on the channel plates. Erickson and Li [22] simulated the transient thermal behavior of an entire microchannel reactor, although they did not consider the temperature dependence of liquid properties. Moreover, the temperature gradient inside the reactor was not due to the Joule heating inside the solution but the solid electric heaters outside the microchannel. Tang et al. [23] investigated the Joule heating effect on the steady state electroosmotic flow in an uncoated capillary, and obtained a significant radial temperature difference under high electric fields (e.g., over 10° in the capillary with a 100-μm internal diameter under a 50-kV m^{-1} electric field). However, they also assumed a uniform electric field. In this work, we will develop a finite element based numerical model to investigate the dynamic effect of Joule heating on the temperature, potential and flow fields during capillary electroosmosis. Variations of material properties with respect to temperature are taken into consideration. In this way, the temperature field, the electrical double layer field, the applied electrical field and the flow field are coupled together. In addition, we will consider a capillary with a finite length and hence consider the thermal end effects. Our goal is to present a comprehensive analysis of the effect of Joule heating on the dynamic electroosmotic flow in a whole capillary system.

2. Mathematical model

Fig. 1 shows the capillary system to be modeled in this work, a capillary joining two reservoirs. The liquid in the reservoirs is assumed to be at the ambient temperature, T_∞. Although both reservoirs, particularly the downstream reservoir, receive heat from the liquid flowing in the capillary, this heat contribution is negligible for reservoir volumes on the order of microlitres. The capillary is composed of three components: liquid domain with a radius R, fused silica wall with a radius R_w and polyimide coating with a radius R_p. The axial length of the capillary is L. In cylindrical coordinates, it reduces to a 2-D problem if the gravity effect (buoyancy induced natural convection) is neglected.

2.1. Governing equations

As has been well discussed in the literature [24–26], electroosmotic flow is governed by the continuity equation

$$\nabla \cdot \mathbf{v} = 0 \tag{1}$$

and the momentum equations subjected to an electrical body force

$$\rho\left[\frac{\partial \mathbf{v}}{\partial t} + (\mathbf{v}\cdot\nabla)\mathbf{v}\right] = -\nabla p + \nabla\cdot[\mu(T)\nabla\mathbf{v}] + \rho_e\mathbf{E}, \tag{2}$$

where $\mathbf{v}$ is the velocity vector, t the time, ρ the density of liquid assumed to be incompressible, p the hydrodynamic pressure, $\mu(T)$ the temperature dependent viscosity with T the absolute temperature, ρ_e the electric charge density, and $\mathbf{E}$ the externally applied electric field.

The electric charge density is related to the internal potential field ψ of the electric double layer (EDL), formed by the charge at the capillary internal wall or the so-called zeta potential ζ, by the Poisson equation [1]

$$\nabla\cdot\left[\frac{\varepsilon(T)}{\varepsilon_{ref}}\nabla\psi\right] = -\frac{\rho_e}{\varepsilon_0\varepsilon_{ref}}, \tag{3}$$

where $\varepsilon(T)$ is the temperature dependent dielectric constant, ε_{ref} the reference dielectric constant, and ε_0 the permittivity of the vacuum. For a symmetric electrolyte solution, say KCl, ψ is determined by the Poisson–Boltzmann equation

$$\nabla\cdot\left[\frac{\varepsilon(T)}{\varepsilon_{ref}}\nabla\psi\right] = \kappa^2\sinh\left(\frac{z_v e\psi}{K_B T}\right), \tag{4}$$

$$\kappa = \left(\frac{2n_0 z_v^2 e^2}{\varepsilon_{ref}\varepsilon_0 K_B T}\right)^{1/2}, \tag{5}$$

where κ^{-1} is the characteristic thickness of the EDL with n_0 the bulk ionic concentration, z_v the valence, e the electron charge and K_B the Boltzmann's constant, respectively.

The electric field $\mathbf{E}$ is calculated from the externally applied electric potential ϕ by

$$\mathbf{E} = -\nabla\phi. \tag{6}$$

Since the capillary wall is non-conducting, the conservation of electric current gives

$$\nabla\cdot[\sigma(T)\nabla\phi] = 0, \tag{7}$$

where $\sigma(T) = \lambda(T)C$ is the temperature dependent electric conductivity with C the molar concentration and $\lambda(T)$ the molar conductivity of the solution, respectively. The molar concentration is dependent on the bulk ionic concentration n_0 in Eq. (5) by $n_0 = N_a C$ with N_a the Avogadro's number.

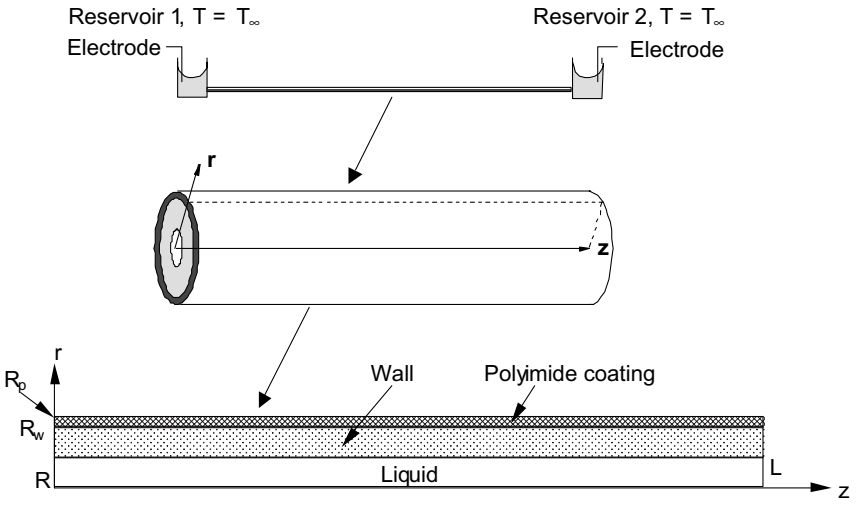

Fig. 1. The capillary system to be modeled and the computational domain.

While the flow field in Eq. (2), EDL potential field in Eq. (4), and applied electric potential field in Eq. (7) are all restricted in the liquid region, the temperature field must be extended to cover the whole computational domain (see Fig. 1). Within the liquid region, the energy equation in the presence of electroosmotic flow effect is given by

$$\rho C_p\left(\frac{\partial T}{\partial t}+\mathbf{v}\cdot\nabla T\right)=\nabla\cdot[k(T)\nabla T]+\sigma(T)\mathbf{E}\cdot\mathbf{E}, \tag{8}$$

where C_p is the specific heat of the liquid and is assumed to be constant in this work, $k(T)$ the temperature dependent thermal conductivity. Here, we have neglected the term associated with viscous dissipation (i.e., the thermal energy converted from the mechanical energy) because it is small compared to the Joule heat. Within the two solid regions, the energy equations become

$$\rho_{\mathrm{w}}C_{p\mathrm{w}}\frac{\partial T}{\partial t}=\nabla\cdot[k_{\mathrm{w}}(T)\nabla T], \tag{9}$$

$$\rho_{\mathrm{p}}C_{p\mathrm{p}}\frac{\partial T}{\partial t}=\nabla\cdot[k_{\mathrm{p}}(T)\nabla T], \tag{10}$$

where the subscripts "w" and "p" denote the capillary wall and polyimide coating, respectively.

2.2. Modeling simplifications

It is rather difficult to solve the set of Eqs. (2), (4) and (7)–(10) without simplifications. The main problem lies in the simultaneous presence of three separate length scales: the capillary length of millimeters, the capillary radius of micrometers and the EDL thickness of nanometers. A complete solution on all the three length scales would require a prohibitive amount of memory and computational time. Therefore, two methods have been proposed to solve this problem. One is to artificially increase the order of magnitude of the EDL thickness, and a qualitative nature of the flow field can thus be obtained [24,25]. The other way is to apply a slip boundary condition at the wall, and avoid the solution of the EDL field (i.e., Eq. (4)) [26,27]. In this work, the second approach is chosen, where the liquid at the capillary internal wall is assumed to slip at a velocity $V_{\mathrm{wall}}=\mu_{eo}E_z$ with $\mu_{eo}=-\varepsilon(T)\varepsilon_0\zeta(T)/\mu(T)$ the electroosmotic mobility and E_z the local electric field in the axial direction (the axial coordinate z is indicated in Fig. 1).

Another simplification is made with respect to the momentum equations. Since electroosmotic flows are generally limited to small Reynolds numbers, the convection term (i.e., the second term on the left hand side) in Eq. (2) can be neglected [22,27]. In addition, it has been shown that the characteristic time t_{steady} for an electroosmotic flow to reach the steady state is on the order of milliseconds [24,26], which is far less than the characteristic time of thermal diffusion in this system (on the order of seconds) [28]. Hence, we can reasonably omit the transient term in the momentum equations as long as the time step sizes selected in the numerical simulation are greater than t_{steady} [26].

Finally, the set of non-dimensional equations determining the applied electric potential field, flow field, and temperature field is summarized as

$$\left.\begin{aligned}
&\nabla\cdot\left[\frac{\sigma(\Theta)}{\sigma_{\mathrm{ref}}}\nabla\Phi\right]=0\\
&\nabla\cdot\mathbf{V}=0\\
&0=-\nabla P+\nabla\cdot\left[\frac{\mu(\Theta)}{\mu_{\mathrm{ref}}}\nabla\mathbf{V}\right]\\
&\frac{\partial\Theta}{\partial\tau}+P_e\mathbf{V}\cdot\nabla\Theta=\nabla\cdot\left[\frac{k(\Theta)}{k_{\mathrm{ref}}}\nabla\Theta\right]+\frac{\sigma(\Theta)}{\sigma_{\mathrm{ref}}}\nabla\Phi\cdot\nabla\Phi\\
&\frac{\rho_iC_{pi}}{\rho C_p}\frac{\partial\Theta}{\partial\tau}=\nabla\cdot\left[\frac{k_i(\Theta)}{k_{\mathrm{ref}}}\nabla\Theta\right]
\end{aligned}\right\}, \tag{11}$$

where the length is scaled by the capillary internal diameter (i.e., $2R$ in Fig. 1), $\Phi=\phi/\varphi$ with φ the potential applied at the capillary inlet, $\mathbf{V}=\mathbf{v}/V_{\mathrm{ref}}$ with the reference velocity, $P_e=\rho C_pRV_{\mathrm{ref}}/k_{\mathrm{ref}}$ the Peclet number, $V_{\mathrm{ref}}=\varepsilon_{\mathrm{ref}}\varepsilon_0\zeta_{\mathrm{ref}}\varphi/\mu_{\mathrm{ref}}L$, $P=p/\rho V_{\mathrm{ref}}^2$, $\tau=tk_{\mathrm{ref}}/\rho C_pR^2$ and $\Theta=(T-T_\infty)k_{\mathrm{ref}}/\varphi^2\sigma_{\mathrm{ref}}$. The subscript i may be "w" for the capillary wall or "p" for the polyimide coating.

We now specify the boundary conditions for the problem. For the applied electric field, we impose insulation conditions along the edges of the liquid domain, and non-dimensional values of 1 at the inlet and 0 at the outlet of the capillary. For the flow field, we impose fully developed velocity profiles at both ends of the capillary, a symmetric condition along the axis, and a slip velocity along the charged wall. For the temperature field, we impose isothermal conditions at both ends of the capillary, a symmetric condition along the axis, and a convective boundary condition surrounding the capillary given by

$$\left[\frac{\partial\Theta}{\partial r}+\frac{h}{k_{\mathrm{p}}(\Theta)}\Theta\right]_{r=R_{\mathrm{p}}}=0, \tag{12}$$

where h is the convective heat transfer coefficient, and the radial coordinate r is indicated in Fig. 1.

2.3. Numerical method

The equations in (11) were solved through the finite element method using an in-house written code. We employ 6-noded quadratic triangle elements for the electric potential, velocity and temperature, and 3-noded linear triangle elements for the pressure. A non-uniform grid is generated with grid refinement along the axial direction in the regions near the capillary inlet and outlet, where field variables were found to vary most

strongly. At each time step, we use properties evaluated with the current temperature field (initially at room temperature), to determine in turn the potential field, wall slip velocity and flow field. Next, known values of potential and velocity fields are used to solve for the new temperature field at the current time step. These steps are repeated until the temperature variation between adjacent time steps is less than a tolerance (i.e., attain a steady state) or a prescribed time is exceeded for those cases where steady state is inaccessible (i.e., a thermal runaway [19,20]).

To verify the code, we consider two test cases for which analytical solutions are available: One is the homogeneous electroosmotic flow in a cylindrical capillary considered by Rice and Whitehead [29], and the other is the 1-D heat conduction across a cylindrical capillary considered by Gobbie and Ivory [19]. Our results are in good agreement with these analytical formulae.

3. Results and discussion

We assume that the liquid has similar physical properties as water, and all the material properties used in the simulation are summarized in Table 1. The dimensions and properties of the flexible fused silica capillary tubes used in this work are provided by Polymicro Technologies, USA [30]. The outer diameter of the capillary is 360 μm with a 20-μm thick polyimide coating (i.e., $R_w = 160$ μm and $R_p = 180$ μm). The capillary internal radius, R, was a parameter in the simulation.

3.1. General features

3.1.1. Temperature field

Fig. 2 shows the transient development of the temperature field. We see that as time goes on, the temperature of the whole capillary is elevated (Fig. 2a). But, temperature gradients are mainly in the inlet and outlet regions. The inlet region is gradually expanded while the outlet region is shortened. These dynamic changes are due to the advective effect of electroosmotic flow, which continuously pulls the cold solution from the inlet reservoir while pushes the hot solution into the outlet reservoir. The temperature difference between the capillary core and the ambient is very small (Fig. 2b). It is attributed to the high Biot number of the whole system. The radial temperature gradient, however, might be significant due to the essentially small capillary radius. We will discuss the effects of radial and axial temperature gradients in the next section.

3.1.2. External potential field

Fig. 3 shows the transient development of the axial electric field E_z, which has been scaled by φ/L (i.e., the nominal electric field applied to the capillary, E_{nom}). Initially, E_z is uniform because the liquid temperature is uniform. When temperature gradients arise in the inlet and outlet regions, the axial electric field is altered. The higher the temperature is, the larger the local electric conductivity becomes, resulting in a lower local electric field intensity. As shown in the figure, the electric field is highly non-uniform near the entrance and exit of the capillary. This non-uniformity is the main difference between the current full model and the solid "solution" model we mentioned above, which will be further discussed in the next section.

3.1.3. Flow field

Fig. 4 shows the transient development of the electroosmotic velocity. The electroosmotic velocity is gradually increased over time as the temperature rises (Fig. 4a). Another important finding is the convex velocity profile at the middle of the capillary (Fig. 4b), resulting from the velocity difference between the electroosmotic wall velocity and the bulk liquid motion. This velocity profile shape is caused by an induced pressure field. Because of the temperature difference along the capillary, the electroosmotic flow velocity is different along the capillary length direction as well. Therefore, an induced pressure filed exists inside the capillary along the flow direction to adjust the axial flow velocity in order to satisfy the continuity equation (i.e., the constant flow rate). Fig. 5 shows the sine-like

Table 1
Material properties used in the simulation

	Liquid	Capillary wall	Coating
Density, $\rho \times 10^3$ (kg m^{-3})	1.00*	2.15*	1.42
Heat capacity, $C_p \times 10^3$ (J kg^{-1} K^{-1})	4.18*	1.00*	1.10
Thermal conductivity, k (W m^{-1} K^{-1})	$0.61 + 0.0012(T - T_\infty)$*	$1.38 + 0.0013(T - T_\infty)$*	0.15
Molar conductivity, $\lambda \times 10^{-3}$ (m^2 S mol^{-1})	$12.64[1 + 0.025(T - T_\infty)]$		
Dynamic viscosity, μ (kg m^{-1} s^{-1})	$2.761 \exp(1713/T) \times 10^{-6}$		
Dielectric constant, ϵ	$305.7 \exp(-T/219)$		

T_∞ is chosen as 298 K in this work.
The properties with the superscript * are obtained from Ref. [31], and those without the superscript * are from Refs. [8] and [9].

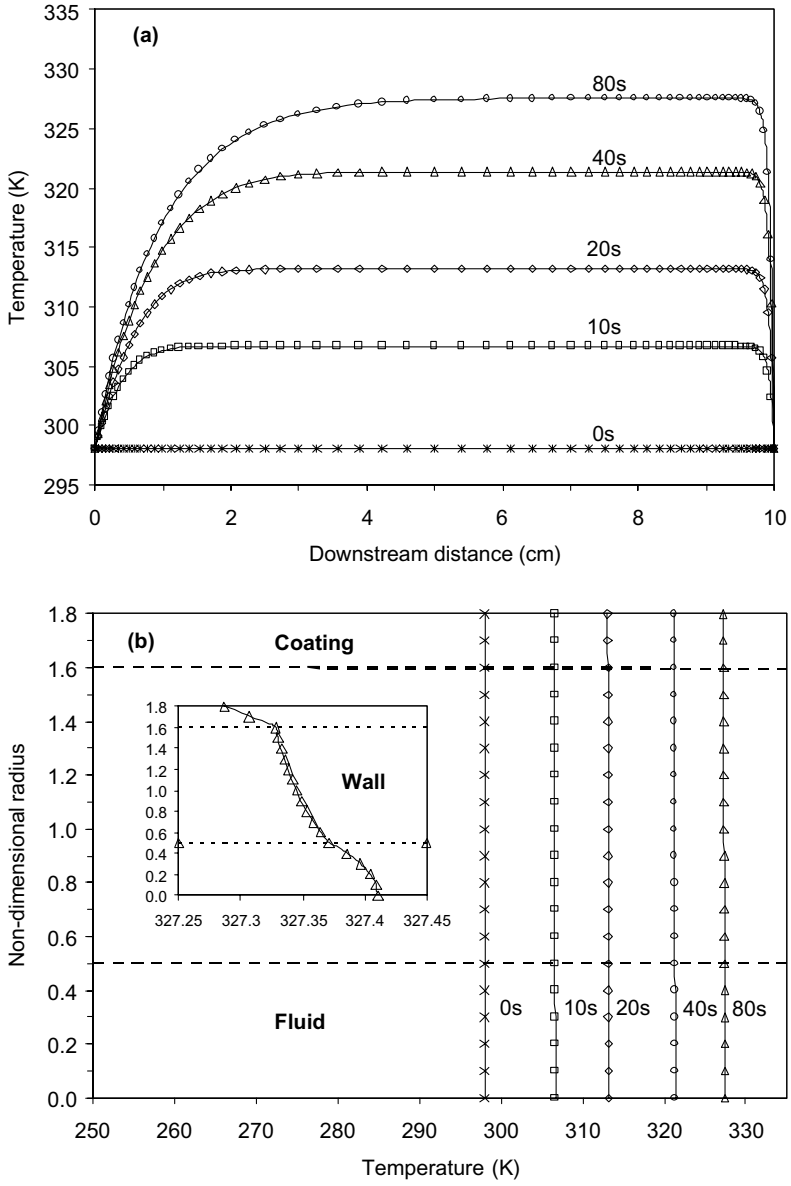

Fig. 2. Transient development of temperature field: (a) along the axis, (b) at the middle of the capillary. The inset in (b) is the expanded view of the temperature profile 80 s after the voltage is applied. Working parameters include internal radius $R = 50$ μm, length $L = 10$ cm, zeta potential $\zeta = -50$ mV, molar concentration $C = 10$ mM, applied electric field 15 kV m^{-1} and heat transfer coefficient $h = 10$ W m^{-2} K^{-1}.

pressure field throughout the capillary. In both the inlet and outlet regions, a positive pressure gradient (pressure increases in the flow direction) is induced to decrease the bulk liquid velocity, while a negative pressure gradient is induced through the rest channel to increase the bulk liquid velocity. Fig. 6 shows the velocity vector plot 80 s after the voltage is applied. We can see a concave velocity profile at both ends of the capillary (Fig. 6a and c), and a nearly flat velocity profile (as we have discussed above, it is actually of convex shape) through most portion of the channel (Fig. 6b).

In summary, the Joule heating effect induces axial temperature gradients in the regions near the capillary inlet and outlet, which in turn change the local electric field and thus the local electroosmotic velocity. These end effects affect the velocity profile through the channel by the conservation of mass requirement.

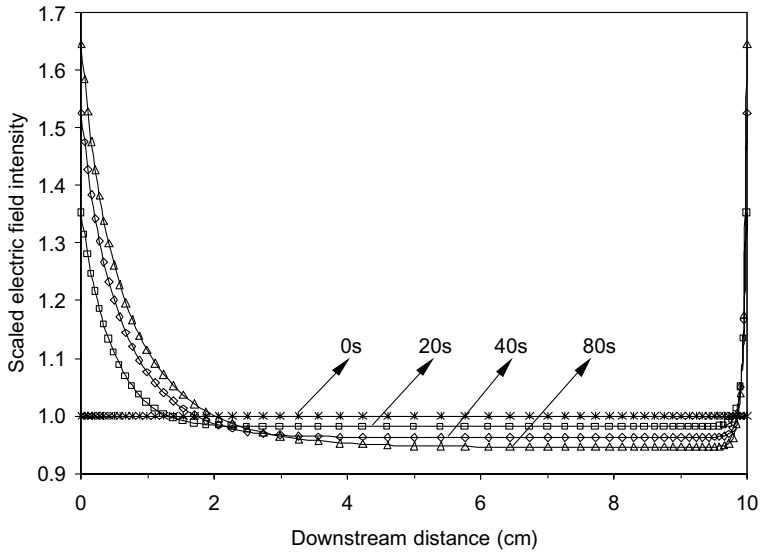

Fig. 3. Transient development of axial electric field. Working parameters are the same as those in Fig. 2.

3.2. Comparison with "solid" solution models

We also calculated the temperature field using the "solid" solution models with and without including the temperature dependence of electric conductivity. Fig. 7 shows the comparison of temperature contours in the whole domain 80 s after the voltage is applied. The "solid" solution models always give a symmetric temperature profile due to the absence of advective flow effects. With the present full model, the electroosmotic flow pushes the high temperature plateau downstream in the capillary. [1] Moreover, we see that the Joule heating effect is significantly underestimated if the temperature dependence of the electric conductivity is neglected. When we use the "solid" solution model to consider this temperature dependence, however, the Joule heating effect is overestimated. Our results agree qualitatively with the experimental observations from Gobbie and Ivory [19], who also observed that the autothermal model with temperature dependent electric conductivity generally over-predicts the capillary temperature, while the constant-conductivity model under-predicts it. We compared the characteristic time required to reach the steady state for the above three models, as shown in Fig. 8. For the case with constant electric conductivity, the characteristic time is the shortest. Our full model predicts a moderate characteristic time.

[1] Actually, as the time goes on, the length of the high temperature plateau is gradually shortened, and can disappear depending on the channel length and the extent of Joule heating effect. We can see this trend in Fig. 2a.

3.3. Influence of working parameters

In this section, we investigate the effects of working parameters and capillary size on the electroosmotic flow using the full model. These effects are discussed individually below, and shown relative to a general case in Figs. 9 and 10. Fig. 9 shows the curves of centerline liquid velocity against time, and Fig. 10 shows the centerline temperature profiles at $t = 80$ s. The liquid velocity at the center of the capillary is normalized by the nominal value of the applied electric field intensity, E_{nom}.

3.3.1. Capillary size

Here, we consider both the capillary internal diameter and the length. As has been well known, decreasing the capillary internal diameter leads to a less Joule heating (see the rise of liquid velocity in case B compared with case A in Fig. 9). Moreover, the time required to reach the steady state is shortened. We want to point out, however, that the faster thermal relaxation is not solely due to the more effective heat dissipation associated with the smaller diameter. The reason is also attributed to the reduction of total Joule heat inside the capillary. This can be qualitatively explained as follows. Let us consider a simple 1-D heat conduction, and assume that the radial temperature difference can be neglected, then the energy conservation inside a capillary gives

$$2\pi R_{\text{p}} h(T - T_0) = \pi R^2 \sigma(T) E_{\text{nom}}^2, \tag{13}$$

where T can now be viewed as the average temperature of the liquid. Assuming a constant electric

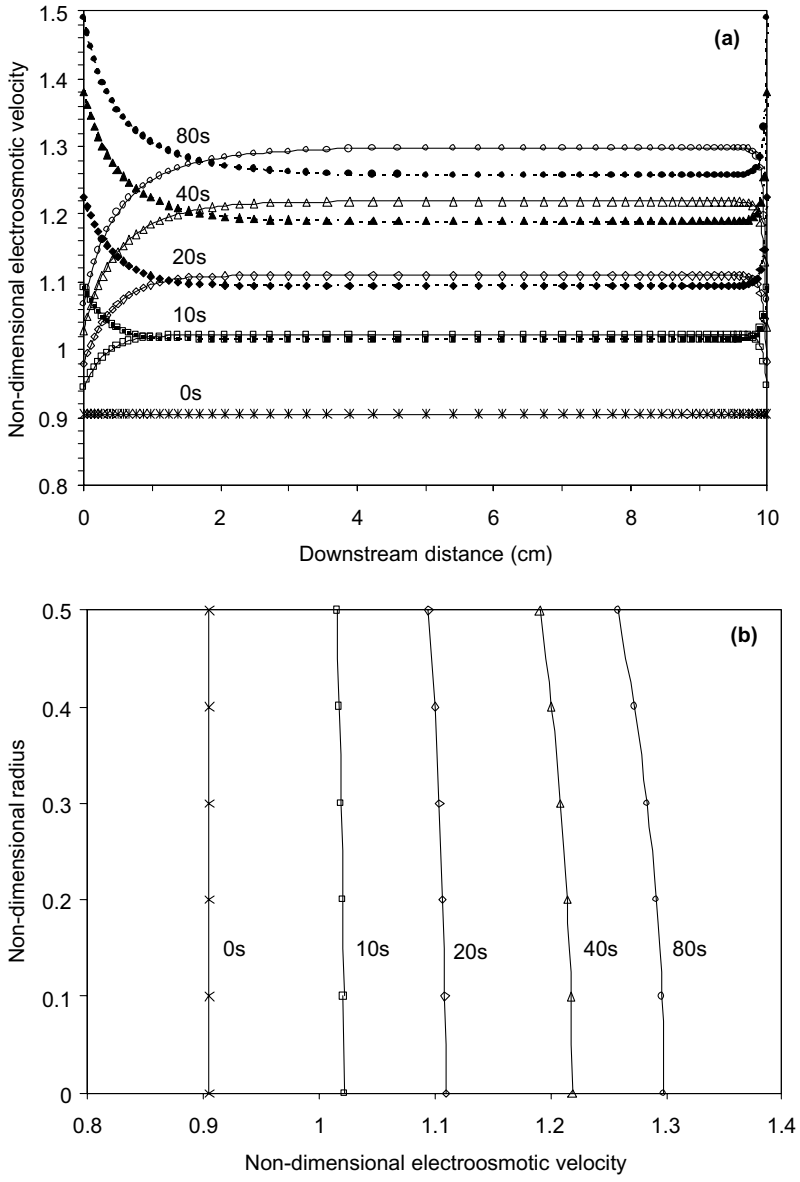

Fig. 4. Transient development of electroosmotic velocity: (a) axial distribution, solid lines with hollow symbols represent the bulk liquid velocity along the axis and dashed lines with full symbols represent the slip velocity along the charged wall (not shown at $t = 0$ s); (b) cross-stream velocity profiles at the middle of the capillary. Working parameters are the same as those in Fig. 2.

conductivity, [2] the temperature elevation, ΔT, of the whole capillary is given by

$$\Delta T = \frac{\sigma (E_{\text{nom}} R)^2}{2 R_{\text{p}} h}, \tag{14}$$

which tells us ΔT is proportional to the square of the capillary internal radius R. Fig. 10 includes the cases where the magnitude of $E_{\text{nom}}R$ holds while R is decreased from 50 μm (case A) to 10 μm (case G). One can see that the temperature differences between cases A and G are relatively small.

The change in the advective flow effect is also noteworthy. For the capillary with a smaller internal radius, the axial temperature profile becomes more symmetric (see case B in Fig. 10), even if the applied electric field is

[2] We also can use the empirical formula for electric conductivity as given in Table 1 to find a more accurate estimation of the whole-capillary temperature rise.

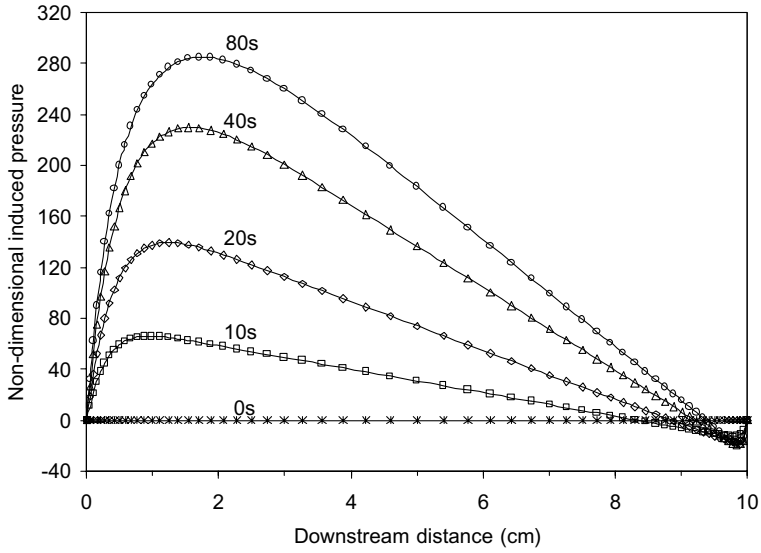

Fig. 5. Transient development of the induced pressure field. Working parameters are the same as those in Fig. 2.

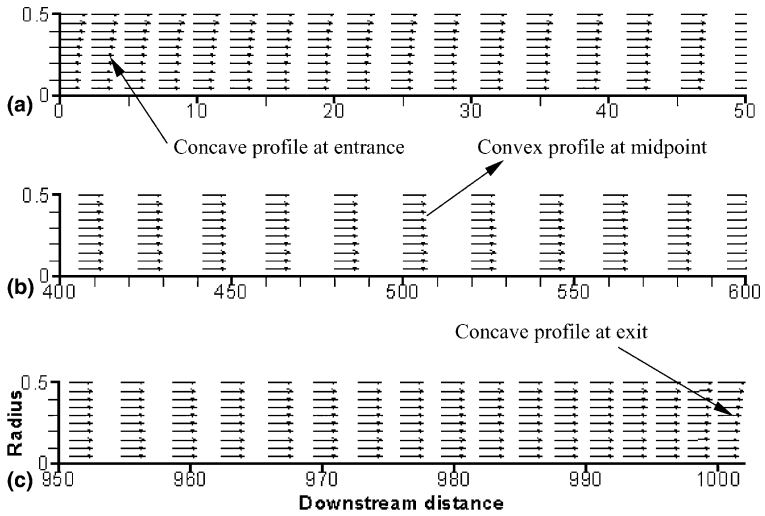

Fig. 6. Velocity vector plot 80 s after the voltage is applied: (a) inlet region; (b) middle region; (c) outlet region. All coordinates are in non-dimensional forms scaled by the capillary internal diameter (100 μm, here). Working parameters are the same as those in Fig. 2.

greatly increased (see case G in Fig. 10) which implies a higher electroosmotic velocity. The two modes of axial heat transport are, respectively, advection and diffusion. As the capillary internal diameter is decreased, the diffusion portion, which is symmetric cooling, is essentially constant. The advection portion that leads to an asymmetric axial temperature profile is, therefore, decreased even at a higher liquid velocity.

For a longer capillary, the role of conductive cooling due to the presence of reservoirs (end effects) is reduced, and the role of convective cooling around the capillary is increased, extending the time to reach the steady state and resulting in higher liquid temperatures. This can be seen from case C compared with case A in Fig. 9. It is also found that the thermal end effects less alter the electroosmotic velocity profile because the induced pressure gradient is less significant in the central portion of a longer capillary.

3.3.2. Applied electric field

From the energy equation (8), we know that the Joule heat is related to the square of the electric field

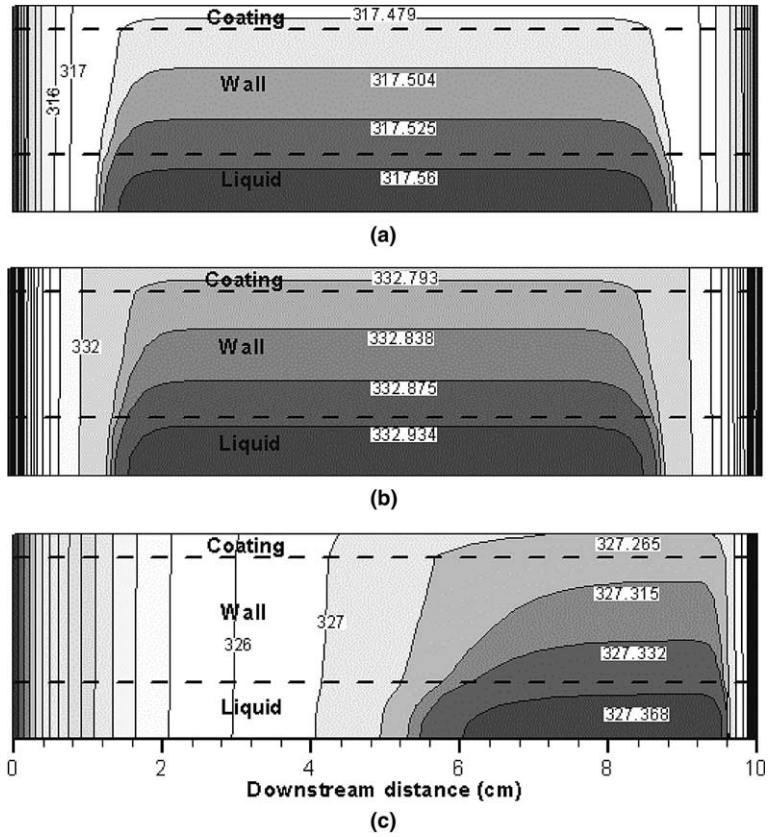

Fig. 7. Temperature contours 80 s after the voltage is applied: (a) "solid" solution model with constant electric conductivity; (b) "solid" solution model with temperature dependent electric conductivity; (c) present full model. The temperature differences between adjacent contour levels are all 2 K except those specially labeled. Working parameters are the same as those in Fig. 2.

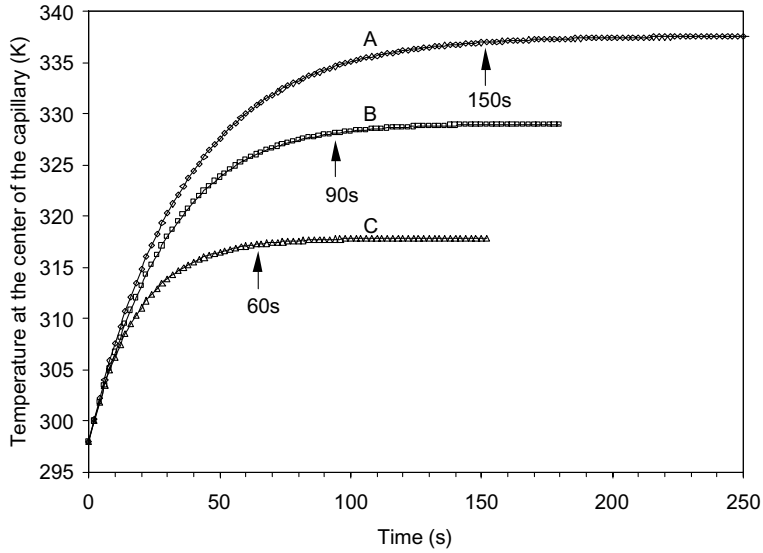

Fig. 8. Transient development of the temperature at the middle point of the capillary along the centerline. Curve A is for the "solid" solution model with temperature dependent electric conductivity; curve B is for the present full model; curve C is for the "solid" solution model with constant electric conductivity. Working parameters are the same as those in Fig. 2.

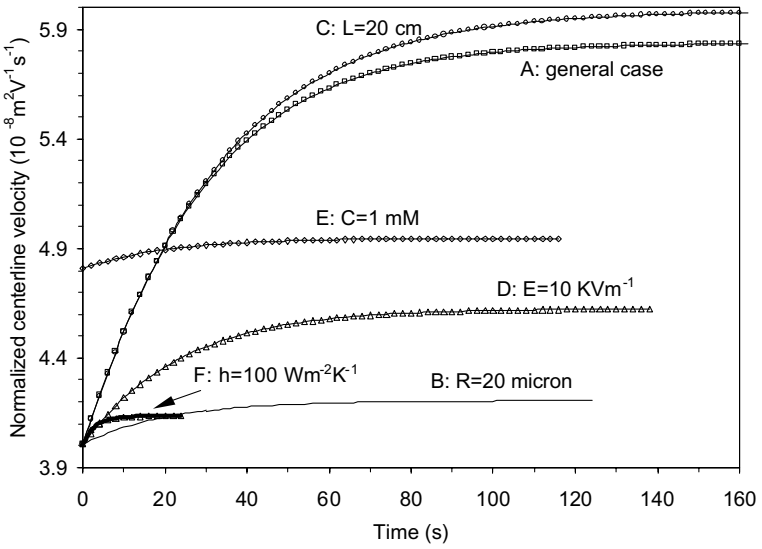

Fig. 9. Comparison of liquid velocity at the middle point of the centerline of the capillary when only one working parameter (with respect to the general case A) is changed for each case, which has been labeled beside the corresponding curve. The velocity is normalized by the nominal electric field intensity. For case E, $\zeta = -60$ mV is used. All other parameters are the same as those in Fig. 2.

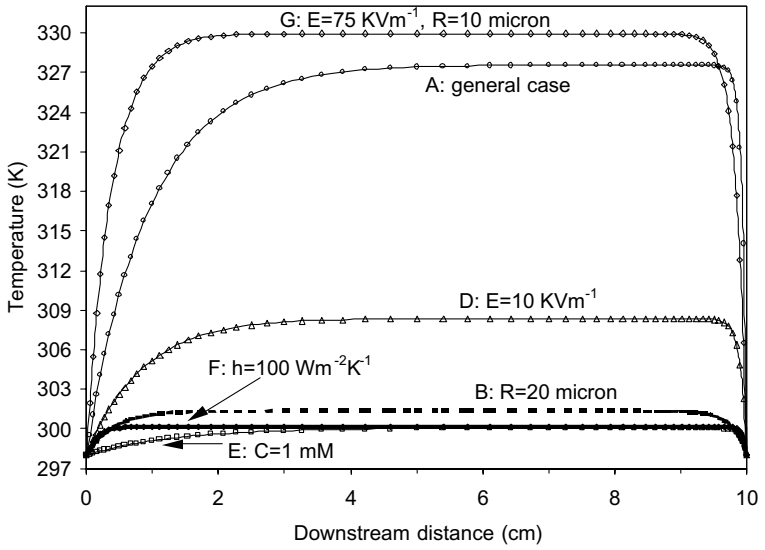

Fig. 10. Comparison of centerline temperature profile 80 s after the voltage is applied when only one working parameter (with respect to the general case A) is changed for each case, which has been labeled beside the corresponding curve. For case E with molar concentration $C = 1$ mM, $\zeta = -60$ mV is used. For case F with heat transfer coefficient $h = 100\ \mathrm{W\,m^{-2}\,K^{-1}}$, the temperature profile is at the time $t = 20$ s. All other parameters are the same as those in Fig. 2.

intensity. A reduced electric field produces less temperature rise, and thus less increase in the bulk liquid velocity and a shorter time to reach the state of thermal equilibrium (see case D compared with case A in Fig. 9). The advective flow effect is reduced as well (see case D in Fig. 10).

3.3.3. Concentration

The molar concentration C determines the solution's electric conductivity by $\sigma(T) = \lambda(T)C$. If the solution is diluted, the electric conductivity is lowered while typically the zeta potential is slightly increased. As a result, the normalized centerline velocity starts at a higher value

than case A, and increases less (see case E in Fig. 9) as time goes on. Due to the reduction in Joule heat generation, the flow effect is similar to the general case (see case E in Fig. 10).

3.3.4. Convective heat transfer coefficient

Improving the capability of heat dissipation will definitely diminish the effect of Joule heating and hence thermal end effects. As shown in Fig. 9, the liquid attains a low, steady state velocity very quickly when the heat transfer coefficient h is increased from 10 $W m^{-2} K^{-1}$ in the general case (case A) to 100 $W m^{-2} K^{-1}$ (case F). Case A corresponds to the free air convection and case F corresponds to the forced air convection. We also see that the temperature field is nearly symmetric (see case F in Fig. 10).

4. Conclusions

We have developed a numerical model to simulate the electroosmotic flow in a full capillary where the Joule heating effect and the thermal end effects are present. The inclusion of temperature dependent liquid properties couples the flow field, the electric potential field and the temperature field. We found that axial temperature gradients result in a non-uniform electric field intensity and thus non-ideal (concave/convex/concave) electroosmotic velocity profiles. Except in the regions near the capillary ends the cross-stream velocity profile is convex. This convex velocity profile is not caused by radial temperature gradients. It is due to the negative pressure gradient induced by reservoir-based thermal end effects. The convex curvature can be diminished by either decreasing the Joule heating effect (e.g., lowering the applied electric field, reducing the capillary internal diameter or reducing the electric conductivity of the solution) or increasing the capillary length. Our results are in qualitative agreement with experimental observations, and showed that previous "solid" solution models either underestimate or overestimate the liquid temperatures.

Acknowledgements

Financial support from the National Sciences and Engineering Research Council (NSERC) of Canada, through a research grant to D. Li is gratefully acknowledged. Financial support from Glynn Williams, through a post-graduate scholarship to D.S. is also gratefully acknowledged. Xuan thanks Chunzhen Ye and David Erickson in Microfluidics Laboratory at Department of Mechanical and Industrial Engineering, University of Toronto for helpful discussions.

References

[1] R.J. Hunter, Zeta Potential in Colloid Science, Principals and Applications, Academic Press, New York, 1981.
[2] J.W. Jorgenson, K.D. Lukacs, Capillary zone electrophoresis, Science 222 (1983) 266.
[3] J. Harrison, K. Fluri, K. Seiler, Z. Fan, C.S. Effenhauser, A. Manz, Micromachining a miniaturized capillary electrophoresis-based chemical analysis system on a chip, Science 261 (1993) 895.
[4] S.C. Jacobson, R. Hergenroder, L.B. Koutny, J.M. Ramsey, High speed separations on a microchip, Anal. Chem. 66 (1994) 1114.
[5] S.V. Ermakov, S.C. Jacobson, J.M. Ramsey, Computer simulations of electrokinetic injection techniques in microfluidic devices, Anal. Chem. 72 (2000) 3512.
[6] E. Grushka, R.M. McCormick, J.J. Kirkland, Effect of temperature gradients on the efficiency of capillary zone electrophoresis separations, Anal. Chem. 61 (1989) 241.
[7] A.E. Jones, E. Grushka, Nature of temperature gradients in capillary zone electrophoresis, J. Chromatogr. 466 (1989) 219.
[8] J.H. Knox, Thermal effects and band spreading in capillary electro-separation, Chromatographia 26 (1988) 329.
[9] J.H. Knox, K.A. McCormack, Temperature effects in capillary electrophoresis. 1: internal capillary temperature and effect upon performance, Chromatographia 38 (1994) 207;
2: theoretical calculations and predictions, Chromatographia 38 (1994) 215.
[10] R.S. Rush, A.S. Cohen, B.L. Karger, Influence of column temperature on the electrophoretic behavior of Myoglobin and α-lactalbumin in high-performance capillary electrophoresis, Anal. Chem. 63 (1991) 1346.
[11] K. Swinney, D.J. Bornhop, Noninvasive picoliter volume thermometry based on backscatter interferometry, Electrophoresis 22 (2001) 2032.
[12] M.E. Lacey, A.G. Webb, J.V. Sweedler, On-line temperature monitoring in a capillary electrochromatography frit using microcoil NMR, Anal. Chem. 74 (2002) 4583.
[13] K.K. Liu, K.L. Davis, M.D. Morris, Raman spectroscopic measurement of spatial and temporal temperature gradients in operating electrophoresis capillaries, Anal. Chem. 66 (1994) 3744.
[14] M. Chaudhari, T.M. Woudenberg, M. Albin, K.E. Goodson, Transient liquid crystal thermometry of microfabricated PCR vessel arrays, J. Microelectromech. Systems 7 (1998) 345.
[15] S.L. Thomson, D. Maynes, Spatially resolved temperature measurements in a liquid using laser induced phosphorescence, J. Fluids Eng. 123 (2001) 293.
[16] D. Ross, M. Gaitan, L.E. Locascio, Temperature measurement in microfluidic systems using a temperature-dependent fluorescent dye, Anal. Chem. 73 (2001) 4117.
[17] D. Erickson, D. Sinton, D. Li, Joule heating and heat transfer in poly(dimethylsiloxane) microfluidic systems, Lab on a Chip 3 (2003) 141.
[18] D. Sinton, D. Li, Electroosmotic velocity profiles in microchannels, Colloid. Surf. A 222 (2003) 273.

[19] W.A. Gobbie, C.F. Ivory, Thermal model of capillary electrophoresis and a method for counteracting thermal band broadening, J. Chromatogr. 516 (1990) 191.
[20] S. Bello, P.G. Righetti, Unsteady heat transfer in capillary zone electrophoresis: I. A mathematical mode, J. Chromatogr. 606 (1992) 95;
II. Computer simulations, J. Chromatogr. 606 (1992) 103.
[21] T.S. Zhao, Q. Liao, Thermal effects on electro-osmotic pumping of liquids in microchannels, J. Micromech. Microeng. 12 (2002) 962.
[22] D. Erickson, D. Li, Numerical simulation of a low power microchannel thermal cycling reactor, Int. J. Heat Mass Transfer 45 (2002) 3759.
[23] G.Y. Tang, C. Yang, J.C. Chai, H.Q. Gong, Joule heating effect on electroosmotic flow and mass species transport in a microcapillary, Int. J. Heat Mass Transfer 47 (2004) 215.
[24] N.A. Patankar, H.H. Hu, Numerical simulation of electroosmotic flow, Anal. Chem. 70 (1998) 1870.
[25] F. Bianchi, R. Ferrigno, H.H. Girault, Finite element simulation of an electroosmotic-driven flow division at a T-junction of microscale dimensions, Anal. Chem. 72 (2000) 1987.
[26] S.V. Ermakov, S.C. Jacobson, J.M. Ramsey, Computer simulations of electrokinetic transport in microfabricated channel structures, Anal. Chem. 70 (1998) 4494.
[27] D. Erickson, D. Li, Influence of surface heterogeneity on electrokinetically driven microfluidic mixing, Langmuir 18 (2002) 1883.
[28] E.V. Dose, G. Guiochon, Timescales of transient processes in capillary electrophoresis, J. Chromatogr. A 652 (1993) 263.
[29] L. Rice, R. Whitehead, Electrokinetic flow in a narrow cylindrical capillary, J. Phys. Chem. 69 (1965) 4017.
[30] From http://www.polymicro.com, homepage of Polymicro Technologies, LLC, USA.
[31] F.P. Incropera, D.P. DeWitt, Fundamentals of Heat and Mass Transfer, Wiley, New York, 1990.